Microlens arrays
with integrated pores

by Shu Yang† and Joanna Aizenberg‡

Microlenses are important optical components that image, detect, and couple light. But most synthetic microlenses have fixed position and shape once they are fabricated, so their possible range of tunability and complexity is rather limited. By comparison, biology provides many varied, new paradigms for the development of adaptive optical networks. Here, we discuss inspirational examples of biological lenses and their synthetic analogs. We focus on the fabrication and characterization of biomimetic microlens arrays with integrated pores, whose appearance and function are similar to highly efficient optical elements formed by brittlestars. The complex design can be created by three-beam interference lithography. The synthetic lens has strong focusing ability for use as an adjustable lithographic mask and a tunable optical device coupled with the microfluidic system. Replacing rigid microlenses with soft hydrogels provides a way of changing the lens geometry and refractive index continuously in response to external stimuli, resulting in intelligent, multifunctional, tunable optics.

†Department of Materials Science & Engineering, University of Pennsylvania,
3231 Walnut Street, Philadelphia, PA 19104, USA
E-mail: shuyang@seas.upenn.edu

‡Bell Laboratories, Lucent Technologies,
600 Mountain Avenue, Murray Hill, NJ 07974, USA
E-mail: jaizenberg@lucent.com

Clear vision is an important adaptation to biological organisms, which in most cases rely on eyes as their photosensory organs for focusing, detection, and imaging. Millions of years of evolution have perfected the design of the lenses used for image formation, resulting in optical structures whose multifunctional and hybrid characteristics are unparalleled in today's technology[1]. For example, the human eye has a flexible lens that changes focus and gain dynamically. In contrast, the muscles in an octopus eye move the lens in and out within the shell to focus on close and distant objects, respectively. An insect eye consists of mesh-like divisions, which split into many identical imaging units called ommatidia. Each ommatidium has a corneal lens that can create a field-of-view (FOV) on its own and vary over an angle. Ommatidia then overlap to provide a composite image of the world to the insect brain. A dragonfly eye contains about 28 000 ommatidia, which cover a 70° horizontal and 90° vertical range of view. Some vertebrates that need to spend their lives in both air and water have developed amphibious eyes, allowing them to see clearly in both media. One particular example is the 'four-eyed fish' *Analeps*, which uses an ovoid lens with different curvatures on different axes, resulting in two focal lengths and two foveas.

Compared with the multifaceted roles of eyes in bio-optics, the attainable range of tunability and complexity in

most technological optical components is rather limited. It would be highly desirable to have complex, robust, and small photonic devices that can mimic the unusual designs and functions seen in biology. A microlens with variable focal length over a wide range is of great interest for increasing the efficiency of light detection, recording, imaging, and coupling. From simple geometrical optics, the focal length f of a thin hemispherical lens can be given by:

$$f = R/(n_2 - n_1) \qquad (1)$$

where R is the lens curvature, n_1 is the refractive index of the surrounding medium, and n_2 is the refractive index of the lens. The focal length of the lens, therefore, is a function of the lens curvature and refractive index contrast. Recently, we developed an electrowetting approach that can dynamically and reversibly change the shape of a liquid microlens by applying a voltage between a conducting liquid and a planar electrode embedded in a dielectric substrate at a certain distance from the liquid-solid interface[2,3]. A different type of tunable fluidic lens is obtained from a thin polydimethylsiloxane (PDMS) membrane sitting on a fluidic chamber bonded to a thin glass slide[4]. Elastic deformation of the membrane occurs when fluid is injected into the lens chamber, mimicking the deformation of lens muscles to change the focal length. A similar approach has been applied to form a convex PDMS lens bonded on a microfluidic chip by varying the pressure in the microfluidic chamber[5,6]. A microdoublet lens consisting of a tunable liquid-filled lens and a solid negative lens has also been investigated[7,8]. The lens can either change shape to biconvex or meniscus, or be filled with a different refractive index liquid, which minimizes optical aberrations and maximizes the tunability of the focal length or FOV.

To mimic the complex nervous and visual systems in octopus eyes, a Si complementary metal-oxide semiconductor (CMOS)-based integrated circuit has been designed and fabricated to process images based on their brightness, size, orientation, and shape[9]. Such electronic vision has the potential to be used in robots for seeing more clearly in dark and murky environments. Artificial ommatidia with a wide FOV can be created using microlens-induced self-writing of polymer waveguides[10]. Each ommatidium consists of a self-aligned microlens, a spacer, and a waveguide, resulting in single-peak angular sensitivity with an acceptance angle comparable to their biological counterparts.

In contrast to the natural optical 'eyed' networks discussed above, no specialized eyes have been documented in brittlestars. However, these organisms exhibit a wide range of photic responses. In a light-sensitive brittlestar, *Ophiocoma wendtii*, we have discovered that the single calcite crystals used for skeletal construction are also a component of the photoreceptor, possibly with the function of a compound eye[11,12]. The periphery of the calcitic skeleton extends into a close-set, nearly hexagonal array of spherical microstructures that display characteristic double lenslets (Fig. 1). The lenses guide and concentrate light onto photosensitive tissue and offer remarkable focusing ability, angular selectivity, and signal enhancement. It is worth noting an interesting feature of this bio-optical structure, i.e. the presence of a pore network surrounding the lenses, which functions as an adaptive optical device with 'transition sunglasses' capability: the lenses guide and concentrate light onto photosensitive
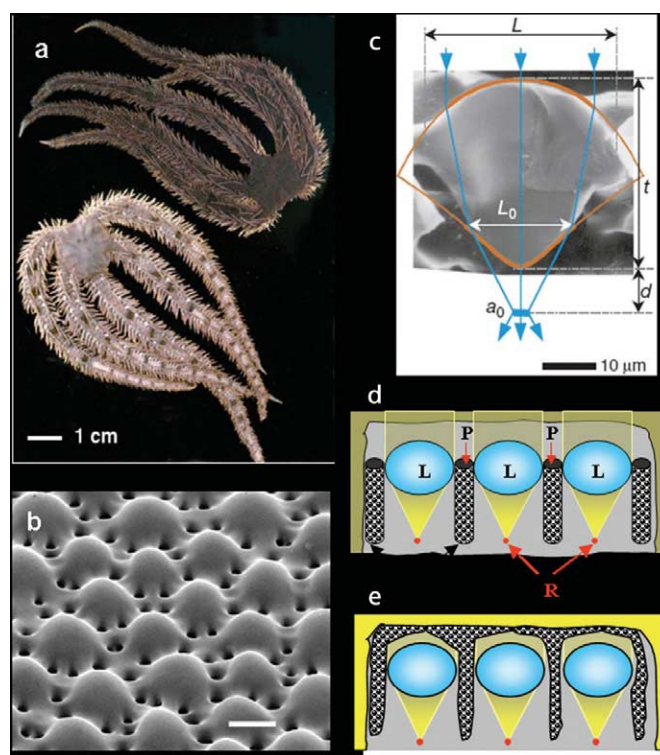

Fig. 1 Structure of a biological microlens array in ophiocomid brittlestars. (a) Light-sensitive species O. wendtii changes color markedly from day (left) to night (right). (b) Scanning electron micrograph (SEM) of a brittlestar lens design (scale bar: 50 µm). (c) SEM of the cross section of an individual lens in O. wendtii. (Reprinted with permission from[11]. © 2001 Nature Publishing Group.) (d-e) Schematics of filtering and diaphragm action of chromatophores: (d) reduced illumination condition (night); (e) illuminated condition (day). CP – pigment-filled chromatophore cell; R – receptor; P – pore; L – lens.

tissue, and the intensity of light reaching the receptors is regulated by the movement of radiation-absorbing intracellular particles through the pores[12]. Thus, the brittlestar microlens arrays can be considered to be an adaptive optical device that exhibits wide-range tunability, including transmission tunability, diaphragm action, numerical aperture tunability, wavelength selectivity, minimization of the 'cross-talk' between the lenses, and improved angular selectivity.

Inspired by the unique lens design and the consequent outstanding optical properties in brittlestars, we have sought novel approaches to create a structure that combines microlens arrays with a surrounding porous microfluidic system. Most existing lens fabrication techniques, including inkjet printing[13], melting of patterned photoresists[14], reactive ion etching of silica and Si[15], soft lithography[16], or self-assembly of monodispersed polymer beads[17], require multiple steps to create both the lens and the pore structures.

Multibeam interference lithography

Multibeam interference lithography has been shown to be a fast, simple, and versatile approach to the creation of periodic porous microstructures that are defect free over a large area[18-20]. When two or more optical waves are present simultaneously in the same region of space, the waves interfere and generate periodic variations in intensity and polarization, which can be transferred into a conventional photoresist film (up to 100 μm thick) to yield periodic lithographic structures with submicron resolution. The photochemistry and lithographic processes involved in multibeam interference lithography are similar to those in conventional techniques, except that photomasks are not required and the substrate is transparent, since the beams are not all necessarily launched from the same side of the substrate. A detailed review of multibeam interference lithography can be found elsewhere[21].

Interference among any n, where $n \leq 4$, noncoplanar laser beams produces an intensity grating with $(n-1)$ dimensional periodicity, if the difference between their wavevectors is noncoplanar. The intensity distribution of the interference field can be described by a Fourier superposition as follows:

$$I(\mathbf{r}) = \sum_{l=1}^{n}\sum_{m=1}^{n} \varepsilon_l \varepsilon_m^* \ \exp i(\mathbf{k}_l - \mathbf{k}_m)\cdot\mathbf{r} \propto \sum_{l=1}^{n}\sum_{m=1}^{n} a_{lm} \exp i\mathbf{G}_{lm}\cdot\mathbf{r} \qquad (2)$$

where r is the position vector, k and ε are the wavevector and polarization vector, respectively, and a_{lm} is the magnitude. The difference between two of the wavevectors, where l,m = 1, 2, ..., n and $l<m$, determines the spatial periodicity, or the translational symmetry, of the interference pattern[22-25]. The combination of Δk_n and ε_n determines the overall symmetry and contrast of the resulting lattice[26-29].

Fabrication of porous, biomimetic lens arrays using three-beam interference lithography

The biological lens arrays in brittlestars appear to be hexagonally packed with surrounding porous structures (Fig. 1). This suggests that it is possible to synthesize a biomimetic analog using three-beam interference lithography through an appropriate arrangement of beams. We therefore set the three beams to have the same wavevectors, k_1 = 2π/a [0.035, 0, 0.999], k_2 = 2π/a [-0.017, 0.03, 0.999], and k_3 = 2π/a [-0.017, -0.03, 0.999], while varying the polarization vectors (see Fig. 2)[30]. When the beams are parallel to each other viewed from the (001) direction (the P1 configuration), a periodic variation of light intensity is generated with hexagonal symmetry and the simulated intensity profile resembles the shape of the biological lens array. In comparison, when the polarization of each wave is perpendicular to the difference between the remaining two wavevectors (the P2 and P3 configurations), a three-fold connectivity with a very small area of highest intensity is observed. This suggests that there is no, or little, lens formation.

By subjecting the interference light to a negative-tone photoresist (SU8), a periodic two-dimensional pattern is obtained that corresponds closely to the calculated light intensity distribution (Fig. 2). The highly exposed regions of the photoresists are crosslinked, making them insoluble in organic developer solution; the unexposed or very weakly exposed regions are dissolved away to reveal holes in the film. In the P1 polarization configuration, when the intensity difference between strongly exposed and adjacent weakly exposed regions is above the threshold, the formation of a lens contour is introduced, creating porous hexagonal microlens arrays that are markedly similar to their biological prototype shown in Fig. 1b. The lens contour can be amplified by factors such as the quantum efficiency of
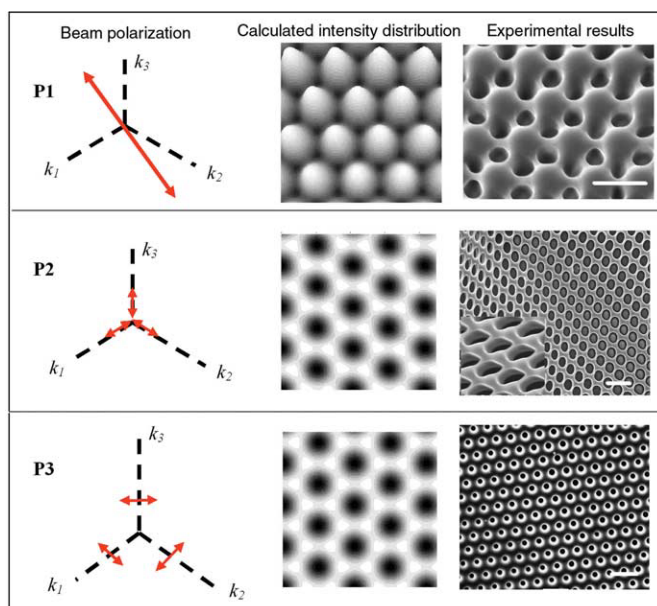
Fig. 2 Two-dimensional structures fabricated by three-beam interference lithography from three different configurations of beam polarizations (shown as double-headed arrows) viewed in the (001) direction. Calculated total intensity distributions (middle) correspond well to the SEM images (right). The brightest region corresponds to the highest intensity of light. An enlarged SEM image is inserted in the P2 polarization to demonstrate a small lens better. Scale bar: 5 µm. (Reprinted with permission from[30]. ©2005 Wiley-VCH.)

Porous lens arrays as multipattern photomasks

The fabricated microlenses show strong focusing ability. Since the biomimetic design combines two imaging elements – microlens arrays and clear windows – in one structure, it offers unique lithographic capabilities as a 'multipattern' photomask.

Photolithographic masks are key components in the fabrication of patterned substrates. Forming the desired structure on the photoresist layer involves passing light through a mask, which has a pattern of opaque chrome regions that blocks portions of the wavefront of the light for each exposure[31]. Different patterns generally require different photomasks, whose total cost is high for multilevel fabrication[32]. Arrays of stacked microlenses can be combined with photomasks in photolithography processing to replicate patterns from photomasks into a photoresist layer[33] or to transfer, for example, macroscopic figures on the mask into multilevel microstructures in the photoresist on a planar substrate in the grayscale reduction lithography process[16,34]. While the latter approach allows control of the size of generated features, only one pattern can be generated from each mask. Since microlenses and clear windows would project different light-field profiles onto a photoresist layer, their integration into one element in the biomimetic lens array offers a new photomask design, allowing direct production of variable microstructures with different sizes in a *single* exposure from a *single* mask. This can be achieved by simply adjusting (i) the illumination dose, (ii) the distance between the mask and the photoresist film, and (iii) the tone of the photoresist[35].

photosensitive molecules (i.e. sensitizers and photoacid generators), the strong nonlinear relationship between the dose, and the polymerizability and solubility contrast of the photoresists, as well as the shrinkage of the resist film during drying. The lens' size, shape, symmetry, and connectivity are controlled by adjusting the beam wavevectors and their polarizations, while the pore size and porosity are varied by the laser intensity and/or exposure time.
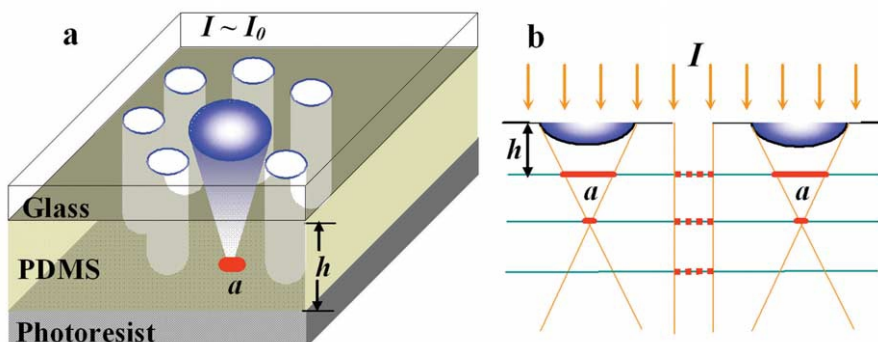

Fig. 3. Biomimetic porous microlens array as a multipattern lithographic photomask: (a) schematic of the experiment; (b) photomask action at different distances, h, from the photoresist and different light intensities I. For I < I_{th}, only features under the lenses are expected (bold red lines). Their size, a, will depend on the distance from the focal point, f. For I > I_{th}, the features under the lenses will be surrounded by the features originating from the pores (dotted red lines). For h > 2f, only features under the windows are expected. (Reprinted with permission from[35]. © 2005 American Institute of Physics.)

A series of microstructures was patterned onto a positive-tone photoresist through the porous microlens arrays, which were then separated by a layer of transparent PDMS with variable thickness (Fig. 3). When the illumination dose I is fixed slightly below the sensitivity threshold I_{th} of the photoresist, no pattern is expected to originate from the light passing through the clear windows, while the focusing activity of the lenses enhances the light field near focus to surpass the resist threshold intensity. For $I < I_{th}$, features in photoresist were generated selectively under the lenses, showing hexagonally packed holes (Figs. 4a and 4b). The size of the features in the resist layer a can be effectively controlled by placing transparent PDMS spacers with different thickness h between the lens and the resist film. For an illumination dose set above the lithographic threshold intensity of photoresist ($I > I_{th}$), patterns were generated that originate from both the lenses and the windows (Figs. 4c and 4d). When $I > I_{th}$ and $h > 2f$, a honeycomb structure was obtained, which originated from the light coming through the pores only (Fig. 4e). The microscale honeycomb structures are of interest as two-dimensional photonic crystals with a large

bandgap. When $I < I_{th}$, and the tone resist is negative (e.g. SU8), hexagonally packed dots were formed, corresponding to the hexagonal lens array in the mask, while their size was reduced (Fig. 4f).

The 'multipattern' lithographic characteristics in the biomimetic lens array were studied quantitatively using simple Fourier optics to simulate the light intensity distribution from both pores and lenses[36]. It was assumed that the pores generated a cylindrical light profile with a peak intensity determined by the illumination dose, and that the lens is diffraction limited at its focus. The calculated three-dimensional profiles of the light field generated by the photomask for $I < I_{th}$, $I > I_{th}$, and at different h values agree well with the corresponding experimental results in Fig. 4[35].

Integrated microfluidic channels for dynamic tuning of optical properties

As discussed earlier, the integration of microlenses and microfluidics offers an attractive route for making a tunable optical device. An electrowetting pump in recirculating fluidic channels has been demonstrated to tune optical fiber properties digitally[37-39]. The electrically controlled and fully reversible motion of fluid plugs in the channels alters the refractive index profile experienced by the optical waveguide modes of the optical fiber.

To mimic the migration of pigment-filled chromatophore cells that regulate the light transmission in a porous brittlestar lens array, a simple microfluidic device was assembled to actuate photoactive liquids within the synthetic microlens array (Figs. 5a and 5b)[30]. When a dye-containing liquid was pumped through the pores, the reduction in light transmission was detected under an optical microscope (Fig. 5c). The percentage of transmission intensity through the lenses can be adjusted, depending on the dye concentration and/or thickness of the dye layer covering the lens. By using different liquids (e.g. with selective refractive index and/or including dyes that can absorb a certain wavelength) as the surrounding medium between the lenses[40], further control over the lens' focal length, numerical aperture, and wavelength selectivity can be introduced. Potential applications include an optical shutter that turns light on and off in an optical interconnect, and autocorrection of the light intensity for spatial vision in bioimaging.
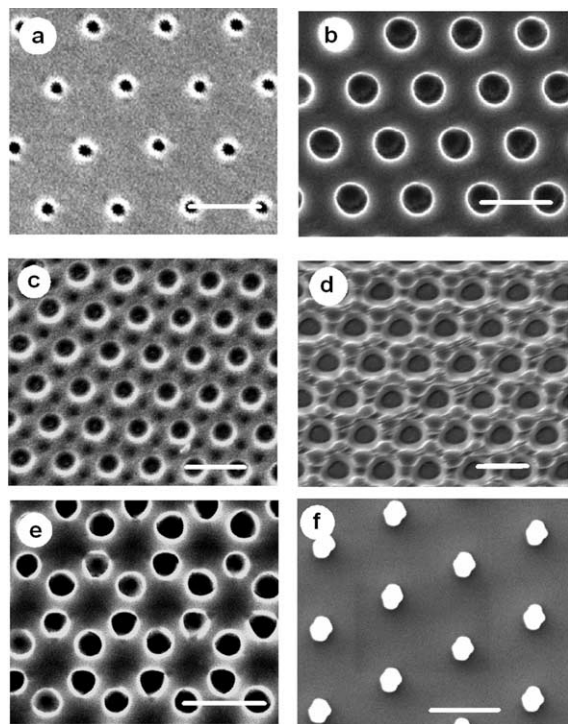

Fig. 4 Examples of photoresist patterns generated using the porous lens arrays as photolithographic masks. (a-e) From positive tone resists (AZ5209) and (f) from a negative tone resist (SU8). (a) $I < I_{th}$, $h \sim f$; (b) $I < I_{th}$, $h < f$; (c) $I > I_{th}$, $h \sim f$; (d) $I > I_{th}$, $h < f$; (e) $I > I_{th}$, $h > 2f$; (f) $I < I_{th}$, $h \sim f$. (Reprinted with permission from[35]. © 2005 American Institute of Physics.)
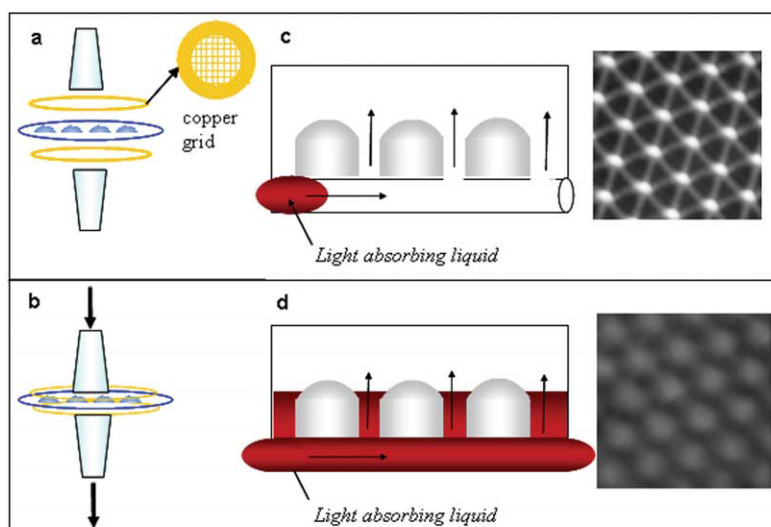
Fig. 5 *Transmission tunability through the lens array using controlled transport of light-absorbing liquid in the channels between lenses: (a) microfluidic assembly and (b) actuation. Light micrographs were recorded in a transmission mode near the focal point (c) without the light-absorbing liquid and (d) with the light-absorbing liquid between the lenses. (Reprinted with permission from[30]. © 2005 Wiley-VCH.)*

Synthesis of soft, biomimetic lens arrays from hydrogels

To provide further tunability of optical properties, it would be highly desirable to replace rigid microlenses with soft structures that could change geometry and refractive index continuously in response to external stimuli, resulting in intelligent, multifunctional optics. The most obvious choice of material for such fabrication is a hydrogel. As elastic polymers, hydrogels are capable of changing their volume and shape by up to several hundred percent in response to pH, temperature, light, electric potential, chemical, and biological agents. They have been used in drug delivery and as tissue scaffolds[41,42], actuators and sensors[43,44] and, most recently, as temperature sensitive lenses[45]. However, most reported hydrogels are prepared from their corresponding liquid monomers by free radical polymerization, which makes them inappropriate for multibeam interference lithography. The inhomogeneity of the radical formation and the lack of control over the radical diffusion in hydrogels has limited resolution to 5 μm. Moreover, radical polymerization from liquids is often accompanied by a large change in volume during crosslinking that often causes swelling and collapse, which are detrimental to the formation of complex structured gels. The use of high-glass-transition-temperature (T_g) polymers that can be crosslinked by a better-controlled photoacids-generation mechanism would improve the film mechanical strength, minimize film roughness, and provide better resolution.

Photoacid-crosslinkable hydrogel precursors that have a high glass transition temperature T_g of ~100°C – i.e. poly(2-hydroxyethyl methacrylate-*co*-methyl methacrylate (PHEMA-*co*-PMMA) – were synthesized for the fabrication of soft, biomimetic microlens arrays[46]. We performed three-beam interference lithography of the hydrogel precursors and fabricated soft, highly deformable hydrogel microlens arrays (Fig. 6). There was almost no change in the unit size of the microlens arrays in the undeformed region, in contrast to the large shrinkage typically observed in radical-polymerized hydrogels. A minimum feature size of 600 nm was achievable.

The use of PHEMA as a hydrogel precursor offers many synthetic and functional advantages. It can be copolymerized with various comonomers to realize different three-dimensional hydrogel structures with tailored architectures, tunability, and functionalities. For example, using responsive hydrogels as microlens materials, we can dynamically tune the lens shape, size, focal length, and/or refractive index to improve the capabilities of rigid structures. We have recently demonstrated a change of focus in response to pH when incorporating 5 mol% poly(acrylic acid) into PHEMA gels[40]. Since the hydrogel precursors are compatible with sol-gel chemistry, it is possible to prepare highly transparent organic-inorganic nanocomposites[47] to improve the mechanical properties of the hydrogel lens without sacrificing its deformability, as well as to increase the refractive index.
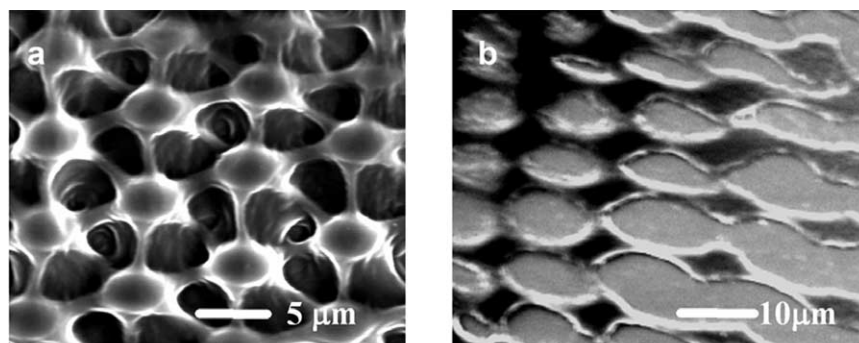
Fig. 6 SEM images of hydrogel microlens arrays formed from PHEMA-co-PMMA: (a) in the nondeformed region; (b) at the edge of the film, where the hydrogel lenses were less crosslinked and not well connected. Here, the lenses were often found stretched and deformed by the capillary force during drying of the developer (methanol). (Reprinted with permission from[46]. © 2005 Royal Society of Chemistry.)

Conclusion

The biological world provides inspirational examples of multifunctional, hybrid optical systems with advanced properties that have led many researchers to try to mimic their structure and function. We have presented fabrication strategies, optical properties, multipattern formation, and tunability of synthetic microlens arrays with integrated pores that mimic the sophisticated microlens arrays evolved by brittlestars. This demonstrates that the lessons learned from nature may improve our current capabilities to construct new, adaptive, microscale hybrid optical devices with multiple functionalities that are potentially useful for a wide variety of technological applications. NT

Acknowledgment

REFERENCES

1. Land, M. F., and Nilsson, D.-E., *Animal Eyes*, Oxford University Press, New York (2002)

2. Krupenkin, T., *et al.*, *Appl. Phys. Lett.* (2003) **82** (3), 316

3. Yang, S., *et al.*, *Adv. Mater.* (2003) **15** (11), 940

4. Zhang, D.-Y., *et al.*, *Appl. Phys. Lett.* (2003) **82** (19), 3171

5. Chen, J., *et al.*, *J. Micromech. Microeng.* (2004) **14** (5), 675

6. Agarwall, M., *et al.*, *J. Micromech. Microeng.* (2004) **14** (12), 1665

7. Chronis, N., *et al.*, *Opt. Exp.* (2003) **11** (19), 2370

8. Jeong, K.-H., *et al.*, *Opt. Exp.* (2004) **12** (11), 2494

9. Gopalan, A., and Titus, A. H., *IEEE Trans. Neural Networks* (2003) **14** (5), 1176

10. Kim, J., *et al.*, *Opt. Lett.* (2005) **30** (1), 5

11. Aizenberg, J., *et al.*, *Nature* (2001) **412**, 819

12. Aizenberg, J., and Hendler, G., *J. Mater. Chem.* (2004) **14** (14), 2066

13. Biehl, S., *et al.*, *J. Sol-Gel Sci. Tech.* (1998) **13** (1-3), 177

14. Haselbeck, S., *et al.*, *Opt. Eng.* (1993) **32** (6), 1322

15. Savander, P., *Opt. Lasers Eng.* (1994) **20** (2), 97

16. Wu, M.-H., *et al.*, *Langmuir* (2002) **18** (24), 9312

17. Lu, Y., *et al.*, *Adv. Mater.* (2001) **13** (1), 34

18. Berger, V., *et al.*, *J. Appl. Phys.* (1997) **82** (1), 60

19. Campbell, M., *et al.*, *Nature* (2000) **404** (6773), 53

20. Yang, S., *et al.*, *Chem. Mater.* (2002) **14** (7), 2831

21. Moon, J. H., and Yang, S., *J. Macromol. Sci. C: Polym. Rev.* (2005) **45** (4), 351

22. Yuan, L., *et al.*, *Opt. Lett.* (2003) **28** (19), 1769

23. Cai, L. Z., *et al.*, *Opt. Commun.* (2003) **224** (4-6), 243

24. Cai, L. Z., *et al.*, *J. Opt. Soc. Am. A* (2002) **19** (11), 2238

25. Cai, L. Z., *et al.*, *Opt. Lett.* (2002) **27** (11), 900

26. Su, H. M., *et al.*, *Phys. Rev. E* (2003) **67** (5), 056619

27. Sharp, D. N., *et al.*, *Phys. Rev. B* (2003) **68** (20), 205102

28. Ullal, C. K., *et al.*, *J. Opt. Soc. Am. A* (2003) **20** (5), 948

29. Ullal, C. K., *et al.*, *Appl. Phys. Lett.* (2004) **84** (26), 5434

30. Yang, S., *et al.*, *Adv. Mater.* (2005) **17** (4), 435

31. Thompson, L. F., *et al.*, *Introduction to microlithography; 2nd edn.*, American Chemical Society, Washington DC, (1994)

32. Nonogaki, S., *et al.*, *Microlithography Fundamentals in Semiconductor Devices and Fabrication Technology*, Marcel Dekker, New York (1998)

33. Völkel, R., *et al.*, *Opt. Eng.* (1996) **35** (11), 3323

34. Wu, H.-K., *et al.*, *J. Am. Chem. Soc.* (2002) **124** (25), 7288

35. Yang, S., *et al.*, *Appl. Phys. Lett.* (2005) **86** (20), 201121

36. Hecht, E., *Optics*, 2nd edn., Addison Wesley, Reading, MA, (1987)

37. Mach, P., *et al.*, *Appl. Phys. Lett.* (2002) **81** (2), 202

38. Hsieh, J., *et al.*, *IEEE Photonics Technol. Lett.* (2003) **15** (1), 81

39. Cattaneo, F., *et al.*, *J. Microelectromech. Sys.* (2003) **12** (6), 907

40. Hong, K., et al., (2005) in preparation

41. Hoffman, A. S., *Adv. Drug Delivery Rev.* (2002) **54** (1), 3

42. Bryant, S. J., and Anseth, K. S., *Biomaterials* (2001) **22** (6), 619

43. Beebe, D. J., *et al.*, *Nature* (2000) **404**, 588

44. Lee, Y. J., and Braun, P. V., *Adv. Mater.* (2003) **15** (7-8), 563

45. Serpe, M. J., *et al.*, *Adv. Mater.* (2004) **16** (2), 184

46. Yang, S., *et al.*, *J. Mater. Chem.* (2005) **15** (39), 4200

47. Kameneva, O., *et al.*, *J. Mater. Chem.* (2005) **15** (33), 3380